Journal of Materials Chemistry A

Accepted Manuscript

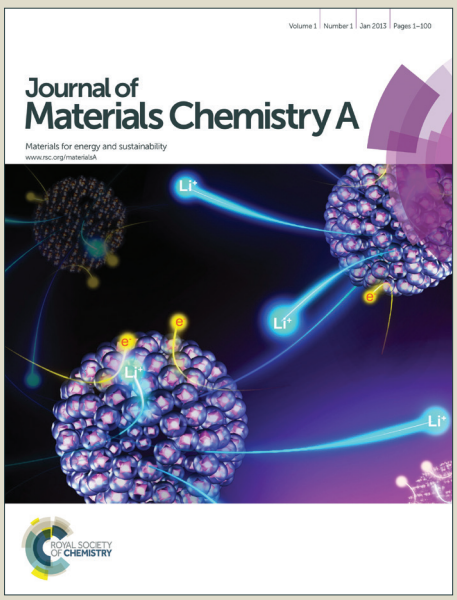

ROYAL SOCIETY OF CHEMISTRY

www.rsc.org/materialsA

Journal of Chemistry A

COMMUNICATION

Agarose-biofunctionalized, dual-electrospun heteronanofiber mats: Toward metal-ion chelating battery separator membranes

Received 00th January 2012,
Accepted 00th January 2012

DOI: 10.1039/x0xx00000x

www.rsc.org/

Ju-Myung Kim, Chanhoon Kim, Seungmin Yoo, Jeong-Hoon Kim, Jung-Hwan Kim, Jun-Muk Lim, Soojin Park*, and Sang-Young Lee*

A facile and efficient way to impart compelling chemical functionality is the utilization of bio-related materials that are easily accessible from natural products. Here, inspired by anomalous physicochemical features and natural abundance of agarose, we demonstrate a new class of agarose-biofunctionalized, dual-electrospun heteronanofiber mat as a chemically-active separator membrane for high-performance lithium-ion batteries. The agarose-enabled metal ion chelation effect of the separator membrane, in combination with its highly-porous structure and superior electrolyte wettability, provides unprecedented improvement in cell performance far beyond those accessible with conventional battery separator membranes.

A forthcoming clean and smart energy era, boosted by the tremendous progress of electric vehicles (EVs) and grid-scale energy storage systems (ESSs), strongly pushes us in pursuit of rechargeable power sources with reliable electrochemical properties and robust safeties.[1,2] Among various energy storage systems, undoubtedly, lithium-ion batteries are a frontrunner, particularly in portable applications. From the viewpoint of ion/electron transport, which crucially affects battery performance, microporous separator membranes (simply separators), in addition to other battery components such as electrodes and electrolytes, should not be underestimated because they allow ionic flow through electrolyte-filled microporous channels and also prevent electrical contact between electrodes.[3,4]

Currently, polyolefin-based microporous separators are widely used in lithium-ion batteries. Despite such commercial popularity, they have intrinsic drawbacks related to porous-structure incompleteness and thermal weakness. A number of approaches have been undertaken to overcome this challenge,[5-8] including ceramic-modified separators, polymeric nonwoven separators, multilayered separators and electrospun fiber separators. Some meaningful improvement in porosity and thermal stability was presented, however, most of the previously reported separators were electrochemically passive.

Taking into account that a diversity of electrochemical reactions occur at electrode-electrolyte interfaces and also separators positioning between electrodes play a key role as an ion-conducting channel, separators bearing unique chemical functionality are expected to provide unprecedented benefits for cell performance, which will become more pronounced with electrochemically-susceptible electrode materials. For example, spinel lithium manganese oxide ($LiMn_2O_4$, LMO)[9,10] has attracted great attention as a promising cathode material owing to its good safety, rate performance and natural abundance, especially for large-scale energy applications such as EVs and ESSs. Despite these advantageous characteristics, practical application of LMO materials to lithium-ion batteries is staggering mainly due to undesired dissolution of Mn^{2+} ions at eleveated temperatures.[11-13] Specifically, the Mn^{2+} ions dissolved from LMO migrate through electrolyte and thus deposit as metallic Mn on anode surface. In addition, the Mn^{2+} ions tend to be reprecipitated as Mn-containing byproducts on LMO surface, resulting in unwanted resistive layers that hinder ionic migration. Eventually, such Mn^{2+} dissolution-triggered electrode contamination/disruption leads to serious capacity fading during charge/discharge cycling. Previous studies on this issue have focused on surface coating/partial cation substitution of LMO materials, functional binders and electrolyte additives.[14-16] Unfortunately, very few works[17,18] were reported with separators, which were based on partial modification of polyethylene (PE) separators (not new

separators exploiting novel structure/chemistry). As a result, high-temperature cycling performances as well as major separator properties (including ionic flow and thermal stability) were marginally improved.

A facile and efficient way to impart compelling chemical functionality is the utilization of bio-related materials that are easily accessible from natural products. Spurred by anomalous chemical/physical features and natural abundance of biomaterials, their application to energy storage systems has been extensively investigated.[19-23] Most of these previous works were devoted to synthesis of new electrode active materials and binders.[19-21] By comparison, little attention was paid to biomaterial-based separators. Cellulose-related separators were solely reported,[22,23] however, the role of cellulose was limited simply as a thermally-stable mechanical framework.

Here, we demonstrate a new class of natural agarose-biofunctionalized heteronanofiber mat as a chemically-active separator for high-performance lithium-ion batteries. Agarose, which is generally extracted from seaweeds and a linear polysaccharide consisting of D-galactose and 3,6-anhydro-L-galactopyranose linked by α-(1→3) and β-(1→4) glycosidic bonds, has been widely used for gel electrophoresis and food products.[24,25] Owing to the unique chemical structure and facile carbonization, agarose has been also explored as an alternative material for battery electrode binders and carbon additives.[26,27] A salient advantage of agarose, from a separator point of view, is the presence of functional groups such as ether (R-O-R) and hydroxyl (-OH) groups,[28,29] which are expected to effectively capture dissolved metal ions. Moreover, agarose is found to provide an excellent electrochemical stability (Supporting Information Fig. S1), as compared to conventional PE separators. To the best of our knowledge, this is the first study to report agarose-biofunctionalized battery separators. Along with the agarose-mediated biofunctionality mentioned above, dual electrospinning strategy is suggested to attain highly-developed porous structure as well as dimensional/mechanical stability of resulting separators. The introduction of dual electrospinning technique, in combination with the rational material design, enables the fabrication of agarose-biofunctionalized, dual-electrospun heteronanofiber mat separators (referred to as "AHM separators") with full-fledged membrane properties, eventually providing a remarkable improvement in cell performance far beyond those achievable with conventional separators.

The AHM separator was fabricated through the dual electrospinning of agarose/polyacrylic acid (PAA) mixture and polyacrylonitrile (PAN) (Fig. 1a). Photographs and a video clip depicting experimental operation of the dual electrospinning process were presented in Supporting Information Fig. S2. More details on the fabrication of the AHM separator were described in the experimental section. Agarose, similar to other polysaccharides, has strong intramolecular hydrogen bonding, which thus fails to form well-defined electrospun nanofiber mat (Fig. 1b). Importantly, its widely/unevenly distributed nonporous region may hamper ionic flow between electrodes. To suppress this self-agglomeration problem of agarose, another functional polymer (here, PAA) was mixed with agarose. PAA has carboxyl groups and is often used as polymeric binders for silicon (Si) anode.[30] The carboxyl groups of

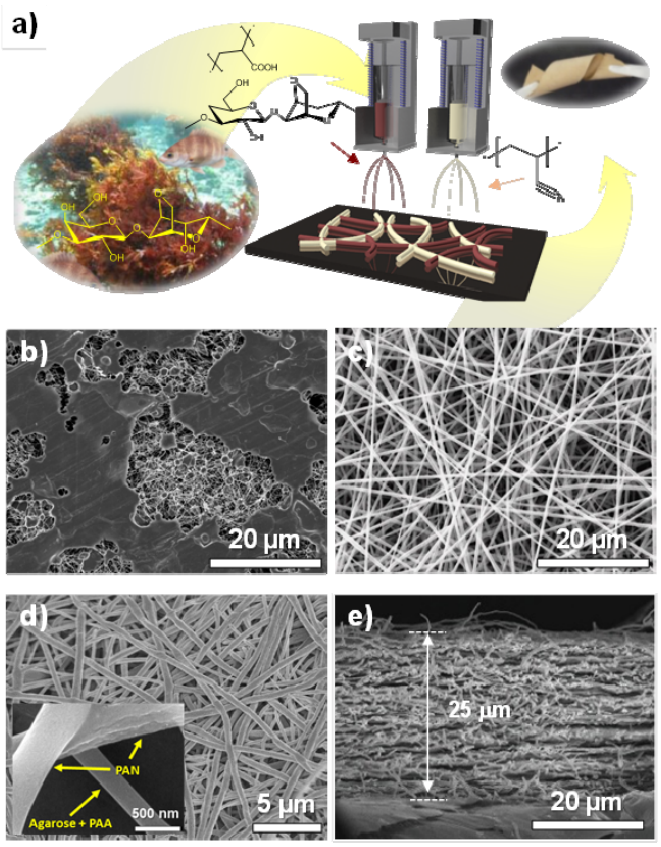

Fig 1. Fabrication and characterization of AHM separator: (a) schematic illustration depicting overall fabrication of AHM separator via dual electrospinning process; (b) SEM image of pristine agarose electrospun nanofiber mat; (c) SEM image of agarose/PAA electrospun nanofiber mat; (d) SEM image of (agarose/PAA)/PAN dual electrospun nanofiber mat (= AHM separator), wherein an inset is high-magnification view; (e) SEM image (cross-sectional) of AHM separator.

PAA are known to establish intermolecular hydrogen bonding with hydroxyl groups of polysaccharides,[31] which could therefore contribute to mitigating the self-agglomeration of agarose nanofibers. The Fourier-transform infrared (FT-IR) spectra (Supporting Information Fig. S3) of the agarose/PAA nanofiber mat show that a broad absorption band at ~ 3330 cm^{-1} (assigned to hydroxyl groups of agarose) is weakened, after being subjected to thermal treatment (= 150 ^{o}C/2 h) that was performed to promote the intermolecular hydrogen bonding. This result demonstrates the thermal condensation reaction between hydroxyl groups of agarose and carboxylic acid moieties of PAA. As a consequence, the agarose/PAA electrospun nanofiber mat suppressed the self-agglomeration of agarose nanofibers, yielding the uniform/spatially-reticulated porous structure (Fig. 1c), where the composition ratio of agarose/PAA was 50/50 (w/w). Other composition ratio did not reach such a well-developed porous structure (Supporting Information Fig. S4).

Although the free-standing nanofiber mat was obtained with the agarose/PAA mixture, its dimensional tolerance upon mechanical deformation (such as wrinkling) was still insufficient to meet

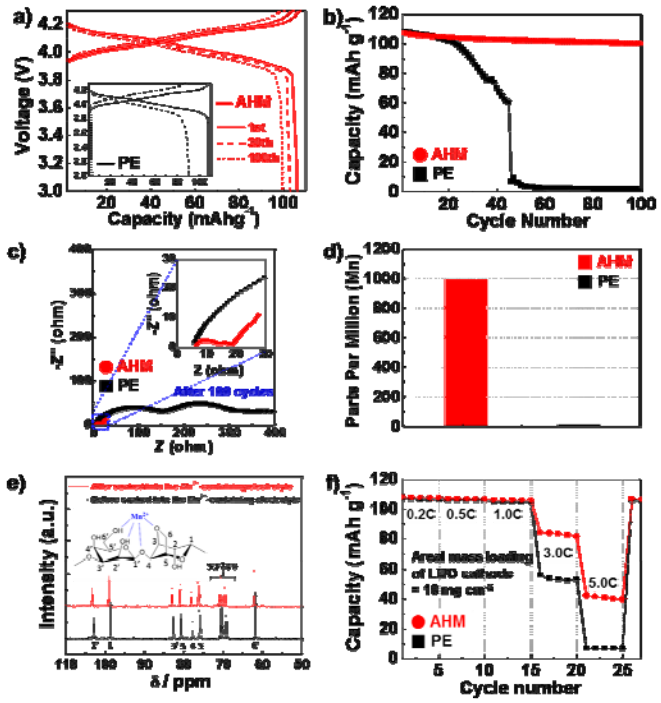

Fig.2 Cell performance of AHM separator (vs. PE separator): (a) charge/discharge profiles with cycling (up to 100 cycles) at 60 °C; (b) high-temperature (60 °C) capacity retention as a function of cycle number; (c) AC impedance spectra after 100 cycles at 60 °C; (d) amount of Mn^{2+} ions captured by separators (estimated from ICP-MS analysis); (e) ^{13}C- NMR spectra verifying the chelation of Mn^{2+} ions by ether/hydroxyl groups of agarose; (f) discharge rate performance for high mass loading LMO cathode (= 18 mg cm^{-2}).

practical requirements of battery separators (Supporting Information Fig. S5a). To resolve this shortcoming, PAN was introduced as a mechanically-reinforcing polymeric framework. Using the dual electrospinning technique, PAN, together with the agarose/PAA nanofibers, was simultaneously electrospun, eventually leading to the (agarose/PAA)/PAN AHM separator with mechanical toughness (Supporting Information Fig. S5b). To further verify this PAN-driven mechanical reinforcement effect, tensile properties of the AHM separator were examined. The stress–strain curves (Supporting Information Fig. S5c) show that the AHM separator presents the higher tensile stress and also the larger elongation at break than the agarose/PAA nanofiber mat. We admit that the tensile properties of the AHM separator are lower than those of the commercial PE separator (Supporting Information Fig. S5d), except for the tensile modulus. Future works will be dedicated to further improving mechanical properties of the AHM separator. Meanwhile, the composition ratio of the AHM separator was identified by estimating the weight change before/after selective etching of water-soluble components (agarose and PAA, prior to the thermal condensation) in water at 50 °C for 12 h. The PAN content was found to be approximately 29 wt.%. From the previous result about the relative composition of agarose/PAA (= 50/50 w/w), the weight-based ratio of the AHM separator led to (agarose/PAA)/PAN = (35.5/35.5)/29 (w/w/w).

Morphological uniqueness of the AHM separator was investigated in detail. A number of heteronanofibers were piled up with being randomly intercrossed (Fig. 1d). Notably, the agarose/PAA nanofibers and PAN ones independently exist (an inset image of Fig. 1d), which was further verified by the energy dispersive X-ray spectroscopy (EDS) analysis of nitrogen (N) element (Supporting Information Fig. S6). The cross-sectional SEM image (Fig. 1e) shows that the average thickness of the AHM separator is approximately 25 μm and also the heteronanofibers are uniformly dispersed over the entire thickness direction.

Porous structure (after being filled with liquid electrolyte) of separators critically affects ion transport between electrodes.[32] The AHM separator, owing to its well-developed pores formed between the heteronanofibers, shows the higher porosity than the PE separator (Supporting Information Table S1 and Fig. S7). This was confirmed by comparing Gurley value (= air permeability) (17 sec 100 cc^{-1} for AHM separator vs. 240 sec 100 cc^{-1} for PE separator) and also ionic conductivity (σ = 0.87 mS cm^{-1} for AHM separator vs. 0.65 for PE separator, after being soaked with 1 M $LiPF_6$ in EC/DEC = 1/1 v/v). In addition, the AHM separator presents the lower McMullin number ($N_M = \sigma_{electrolyte}/\sigma_{separator}$) than the PE separator, indicating that ionic flow through the AHM separator is less hindered due to the well-developed porous structure. Electrolyte wettability of the AHM separator was compared with that of the PE separator. The AHM separator shows the higher electrolyte-immersion height than the PE separator (Supporting Information Fig. S8a), which is attributed to its highly-porous structure and also polar characteristics. Thermal shrinkage test (Supporting Information Fig. S8b) exhibits that the AHM separator, due to its thermally-stable components and no stretching step involved in the separator fabrication, provides better thermal resistance (thermal shrinkage ~ 0 %, after exposure to 150 °C/0.5 h) than the PE separator (~ 95 %). Electrochemical stability of the separators was monitored using linear sweep voltammetry (LSV). No appreciable decomposition of the AHM separator occurred up to 5.0 V (vs. Li/Li^+), which is superior to the PE separator (Supporting Information Fig. S8c). Self-discharge behavior of cells assembled with the AHM separator was examined by measuring open-circuit voltage (OCV) drop as a function of elapsed time. The AHM separator shows a stable OCV profile, which is almost comparable to that of the PE separator (Supporting Information Fig. S8d), demonstrating that the porous structure of the AHM separator was well-tuned against unwanted leakage current between electrodes.

The highly-porous structure and agarose-mediated biofunctionality of the AHM separator are expected to exert beneficial influence on cell performance. The coin cell (2032-type) assembled with LMO cathode (areal mass loading = 12 mg cm^{-2}) and Li metal anode was cycled between 3.0 and 4.3 V at a charge/discharge current density (1.0 C (= 1.52 mA cm^{-2})/1.0 C). The cell containing the AHM separator delivers the stable high-temperature (60 °C) charge/discharge profiles up to 100 cycles (Fig. 2a). By contrast, the cell with the PE separator shows a sharp decay in capacity and also large cell polarization, resulting in the complete loss of electrochemical activity. Notably, the capacity retention after 100 cycles was approximately 93 % for the AHM separator and 0 % for the PE separator (Fig. 2b). This superior capacity retention was

verified by monitoring the variation in the AC impedance spectra of the cells before/after 100 cycles (Fig. 2c, Supporting Information Fig. S9). The growth of the cell impedance after 100 cycles was considerably suppressed in the cell incorporating the AHM separator (Z_{Re} (100th cycle) - Z_{Re} (1st cycle) = $\Delta Z_{Re} \approx$ 12 ohm) compared to that of the cell with the PE separator ($\Delta Z_{Re} \approx$ 300 ohm). This result demonstrates that the AHM separator effectively prevents the formation of undesirable resistive layers predominantly formed on the electrodes.

Such a remarkable improvement in the capacity retention and cell polarization of the AHM separator may be ascribed to the capture of Mn^{2+} ions dissolved from LMO cathode. To prove this hypothesis, the Mn^{2+} chelation ability of the AHM separator was quantitatively investigated by measuring the trapped Mn^{2+} ions after being immersed in manganese perchlorate ($Mn(ClO_4)_2$) electrolyte solution[14] (i.e., 10 mM $Mn(ClO_4)_2$-containing 1.3 M $LiPF_6$ in EC/PC = 1/1 v/v). More details on this analysis were described in the experimental section. The inductively coupled plasma mass spectrometry (ICP-MS) analysis exhibits that the captured Mn^{2+} amount of the AHM separator is almost 50 times higher than that of the PE separator (Fig. 2d). To better elucidate this unique behavior of the AHM separator, pure agarose, PAN and PAA films were respectively prepared as model systems and their Mn^{2+} chelation ability was investigated. Among the three components of the AHM separator, contribution of agarose (137 ppm) to the Mn^{2+} capture was found to be highly noticeable (Supporting Information Fig. S10), in comparison to the PAA (19 ppm) and PAN (7 ppm) that are hardly swollen with the $Mn(ClO_4)_2$ solution. In addition, the change in chemical shift (δ) in ^{13}C-nuclear magnetic resonance (^{13}C-NMR) peaks of the pure agarose film, before/after being soaked into the $Mn(ClO_4)_2$ solution, was examined. Fig. 2e apparently shows the coordination-induced shift[33] of agarose carbon atoms (δ=103.1 (C1'), δ=80.8 (C3), δ=78 (C4), δ=76.3 (C5), δ=70.0 (C6)) bonded to -O-groups and also those (δ=71.0 (C2'), δ=76.08 (C5'), δ=62.1 (C6')) linked to -OH groups, providing the detailed information on chelation of Mn^{2+} ions by ether and hydroxyl groups of agarose. The aforementioned structural analysis demonstrates that the beneficial chelation effect of the AHM separator on the high-temperature cycling performance (i.e., capacity retention and polarization) mainly arises from the biofunctionality of agarose. More in-depth characterization on the high-temperature cycling performance of the AHM separator will be conducted in the following section.

In addition to the cyclability, the AHM separator shows the better discharge rate performance than the PE separator (Supporting Information Fig. S11), where the cells were charged at a constant current density of 0.2 C and discharged at various current densities ranging from 0.2 to 5.0 C. The detailed information on the cell test was provided in the experimental section. Notably, the advantageous effect of the AHM separator on the discharge rate capability became more pronounced at the high mass loading LMO cathode (= 18 mg cm^{-2}, Fig. 2f). This superior rate performance of the AHM separator can be explained by its excellence in ion conductivity (Supporting Information Table S1) and electrolyte affinity (Supporting Information Fig. S8a). The abovementioned beneficial effect of the AHM separator on the cell performance was investigated in great detail, with a particular focus on Mn^{2+} chelation ability.

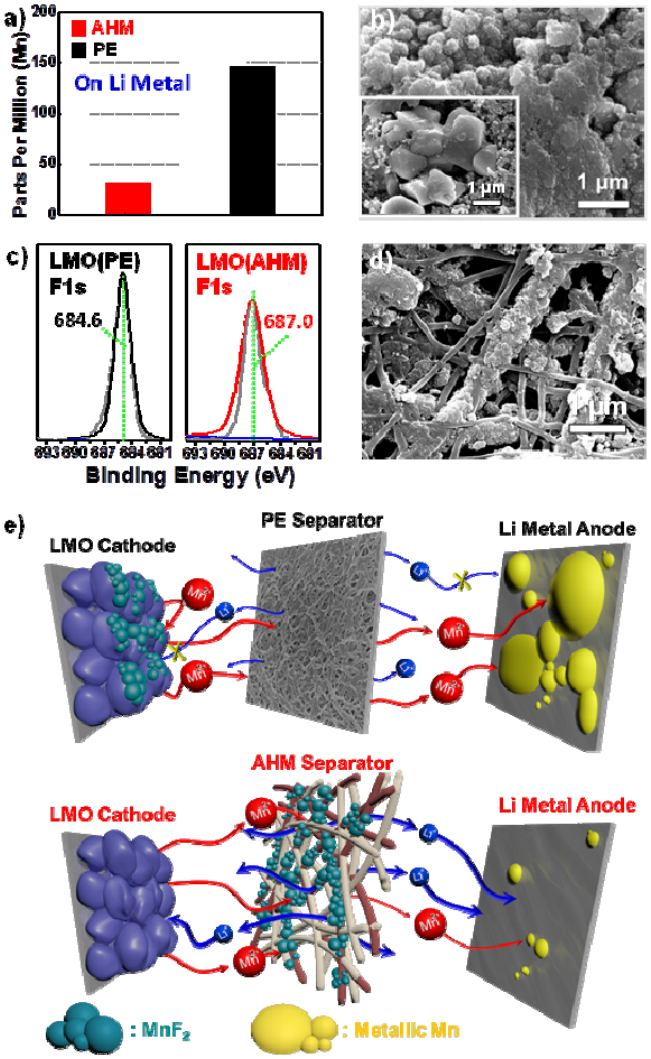

Fig. 3 In-depth analysis of LMO cathode, Li metal anode and separator of cells after 100 cycles at 60 °C: (a) metallic Mn deposited on lithium metal anode (measured by ICP-MS analysis); (b) SEM image of LMO cathode surface assembled with PE separator, wherein an inset shows LMO cathode surface assembled with AHM separator; (c) XPS F 1s spectra of LMO surface; (d) SEM image of AHM separator. (e) A conceptual illustration depicting beneficial effect of AHM separator on high-temperature cycling performance.

After the high-temperature cycling (100 cycles), the cells were disassembled and then surfaces of the lithium metal anode and the LMO cathode were characterized. The metallic Mn deposited on the lithium metal was quantitatively anlayzed using ICP-MS technique (Fig. 3a). In comparison to the PE separator (147 ppm), the AHM separator (32 ppm) significantly suppresses the deposition of metallic Mn on the lithium metal, verifying the Mn^{2+} chelation ability of AHM separator, Fig. 3b shows that the LMO cathode assembled with the PE separator was covered with considerable amount of byproducts.

In comparison, the relatively clean cathode surface was observed at LMO cathode with the AHM separator (an inset image of Fig. 3b). The LMO cathode surface was further examined using the X-ray

photoelectron spectroscopy (XPS) F 1s spectra. For the PE separator, a peculiar peak (684.6 eV) assigned to MnF_2 was observed at the LMO surface (Fig. 3c), revealing that the byproducts shown in the Fig. 3b are associated with MnF_2. The MnF_2 byproducts[34] are known to be formed via unwanted side reactions between dissolved Mn^{2+} ions and hydrofluoric acid (HF, generated from electrolyte decomposition). By contrast, the LMO surface for the AHM separator presents a peak (687.0 eV) corresponding to a typical SEI layer (specifically, $Li_xPO_yF_z$-containing compounds[35]).

Such a dramatic difference in the LMO surface was confirmed by analyzing the AHM separator surface adjacent to the LMO cathode. A large amount of byproducts were formed preferentially along the nanofibers of the AHM separator (Fig. 3d). The XPS Mn 2p and F 1s spectra (Supporting Information Fig. S12) exhibit that the byproducts on the AHM separator surface are ascribed to MnF_2, indicating that the AHM separator effectively captures Mn^{2+} ions during the high-temperature cycling. This beneficial effect of the AHM separator on the cell performance is conceptually illustrated in Fig. 3e. For the PE separator, the Mn^{2+} ions dissolved from LMO cathode tend to deposit as metallic Mn on lithium metal anode and also form MnF_2-containing resistive layer on LMO cathode. By comparison, a significant portion of dissolved Mn^{2+} ions are trapped inside the AHM separator and then turned into MnF_2 on the electrospun nanofibers. Potentially harmful influence of the deposited MnF_2 on ion transport of the AHM separator may not be appreciable due to its highly-developed porous structure, thus little impairing the cell performance.

Conclusions

In summary, inspired by the natural agarose-mediated biofunctionality, we have developed the dual-electrospun (agarose/PAA)/PAN heteronanofiber mat as a new concept of electochemically-active (specifically, metal-ion chelating) battery separator ("AHM separator"). The dual eletrospinning-driven architecturing of the heteronanofiber mat, in combination with the rational tailoring of intermolecular (agarose/PAA) hydrogen bonding, allowed the successful fabrication of the AHM separator. The agarose-enabled Mn^{2+} chelation effect of the AHM separator, along with its highly-porous structure and superior electrolyte wettability, provided unprecedented improvement in the cell performance (in particular, high-temperature cyclability) far beyond those achievable with the conventional PE separator. We envision that the agarose-biofunctionalized AHM separator, owing to the effectiveness/versatility of its metal chelating ability and also full-fledged membrane properties, can be easily combined with a variety of high-voltage/-capacity (but, suffering from metal dissolution) electrode materials, thus boosting up the progress of next-generation high-performance batteries. In addition to the power source applications, it is also anticipated that the AHM separator may hold a great deal of promise as an alternative membrane for use in a wide variety of filtration/purification systems aiming at selective removal of heavy metal ions, which will be a major research theme in our future studies.

Acknowledgements

J.-M. Kim and C. Kim contributed equally to this work. This work was supported by the National Research Foundation of Korea Grant (NRF-2009-C1AAA001-2009-0093307) and Energy Efficiency and Resources R&D program (20112010100150).

Notes and references

Department of Energy Engineering, School of Energy and Chemical Engineering Ulsan National Institute of Science and Technology (UNIST), Ulsan 689–798, Korea E-mail: spark@unist.ac.kr, syleek@unist.ac.kr

† Electronic Supplementary Information (ESI) available: [details of any supplementary information available should be included here]. See DOI: 10.1039/c000000x/

1 M. Armand, J.-M. Tarascon, *Nature* 2008, **451**, 652.
2 V. Etacheri, R. Marom, R. Elazari, G. Salitra, D. Aurbach, *Energy Environ. Sci.*, 2011, **4**, 3243.
3 P. Arora, Z. Zhang, *Chem. Rev.* 2004, **104**, 4419.
4 H. Lee, M. Yanilmaz, O. Toprakci, K. Fu, X. Zhang, *Energy Environ. Sci.* 2014, **7**, 3857.
5 H.-S. Jeong, D.-W. Kim, Y. U. Jeong, S.-Y. Lee, *J. Power Sources* 2010, **195**, 6116.
6 T.-H. Cho, M. Tanaka, H. Ohnishi, Y. Kondo, M. Yoshikazu, T. Nakamura, T. Sakai, *J. Power Sources* 2010, **195**, 4272.
7 E.-S. Choi, S.-Y. Lee, *J. Mater. Chem.* 2011, **21**, 14747.
8 J.-K. Kim, G. Cheruvally, X. Li, J.-H. Ahn, K.-W. Kim, H.-J. Ahn, *J. Power Sources* 2008, **178**, 815.
9 M. S. Whittingham, *Chem. Rev.* 2004, **104**, 4271.
10 O. K. Park, Y. Cho, S. Lee, H.-C. Lee, H.-K. Song, J. Cho, 2011, **4**,1621.
11 J. S. Kim, K. Kim, W. Cho, W. H. Shin, R. Kanno, J. W. Choi, *Nano Lett.* 2012, **12**, 6358.
12 C. Zhan, J. Lu, A. J. Kropf, T. Wu, A. N. Jansen, Y.-K. Sun, X. Qiu, K. Amine, *Nature Commun.* 2013, **4**, 2437.
13 G. Xu, Z. Liu, C. Zhang, G. Cui, L. Chen, *J. Mater. Chem. A* 2015, DOI:10. 1039/C4TA06264G.
14 M.-H. Ryou, S. Hong, M. Winter, H. Lee, J. W. Choi, *J. Mater. Chem. A* 2013, **1**, 15224.
15 M. J. Lee, S. Lee, P. Oh, Y. Kim, J. Cho, *Nano Lett.* 2014, **14**, 993.
16 F. Wu, N. Li, Y. F. Su, L. J. Zhan, L. Y. Bao, J. Wang, L. Chen, Y. Zheng, L. Q. Dai, J. Y. Peng, S. Chen, *Nano Lett.* 2014, **14**, 3550.
17 T. Yim, H.-J. Ha, M.-S. Park, K. J. Kim, J.-S. Yu, Y.-J. Kim, *RSC Adv.* 2013, **3**, 25657.
18 S. H. Woo, H. W. Lim, S. Jeon, J. J. Travis, S. M. George, S. H. Lee, Y. N. Jo, J. H. Song, Y. S. Jung, S. Y. Hong, N. S. Choi, K. T. Lee, *J. Electrochem. Soc.* 2013, **160**, A2234.
19 Y. J. Lee, H. Yi, W. J. Kim, K. Kang, D. S. Yun, M. S. Strano, G. Ceder, A. M. Belcher, *Science* 2009, **324**, 1051.
20 M. Lee, J. Hong, D. H. Seo, D. H. Nam, K. T. Nam, K. Kang, C. B. Park, *Angew. Chem. Int. Ed.* 2013, **52**, 8322.
21 I. Kovalenko, B. Zdyrko, A. Magasinski, B. Hertzberg, Z. Milicev, R. Burtovyy, I. Luzinov, G. Yushin, *Science* 2011, **334**, 75.
22 S.-J. Chun, E.-S. Choi, E.-H. Lee, J. H. Kim, S.-Y. Lee, S.-Y. Lee, *J. Mater. Chem.* 2012, **22**, 16618.

23 J. Zhang, Z. Liu, Q. Kong, C. Zhang, S. Pang, L. Yue, X. Wang, J. Yao, G. Cui, *ACS Appl. Mater. Interfaces* 2013, **5**, 128.
24 J. Guan, B. Wang, S. C. Bae, S. Granick, *J. Am. Chem. Soc.* 2013, **135**, 6006.
25 Y. Li, X. Feng, W. Du, Y. Li, B.-F. Liu, *Anal. Chem.* 2013, **85**, 4066.
26 C. Kim, J. Y. Jang, N.-S. Choi, S. Park, *RSC Adv.* 2014, **4**, 3070.
27 G.-P. Kim, S. Park, I. Nam, J. Park, J. Yi, *J. Mater. Chem. A* 2013, **1**, 3872.
28 L. Yang, W. Tian, Y. Xu, Y. Su, S. Gao, Z. Wang, S. Weng, C. Yan, J. Wu, *J. Inorg. Biochem.* 2004, **98**, 1284.
29 H. Hu, J. Xue, X. Wen, W. Li, C. Zhang, L. Yang, Y. Xu, G. Zhao, X. Bu, K. Liu, *Inorg. Chem.* 2013, **52**, 13132.
30 A. Magasomslo, B. Zdyrko, I. Kovalenko, B. Hertzberg, R. Burtovyy, C. F. Huebner, T. F. Fuller, I. Luzinov, G. Yushin, *ACS Appl. Mater. Interfaces* 2010, **2**, 3004.
31 Y. K. Jeong, T. W. Kwon, I. Lee, T. S. Kim, A. Coskun, J. W. Choi, *Nano Lett.* 2014, **14**, 864.
32 J.-H. Kim, J.-H. Kim, K.-H. Choi, H. K. Yu, J. H. Kim, J. S. Lee, S.-Y. Lee, *Nano Lett.* 2014, **14**, 4438.
33 P. Klüfers, T. Kunte, *Angew. Chem. Int. Ed.* 2001, **40**, 4210.
34 S.-T. Myung, K. Izumi, S. Komaba, H. Yashiro, H. J. Bang, Y.-K. Sun, N. Kumagai, *J. Phys. Chem. C* 2007, **111**, 4061.
35 K. Edström, T. Gustafsson, J. O. Thomas, *Electrochim. Acta* 2004, **50**, 397.

Table of contents

Agarose-biofunctionalized, dual-electrospun heteronanofiber mats: Toward metal-ion chelating battery separator membranes

Ju-Myung Kim, Chanhoon Kim, Seungmin Yoo, Jeong-Hoon Kim, Jung-Hwan Kim, Jun-Muk Lim, Soojin Park*, and Sang-Young Lee*

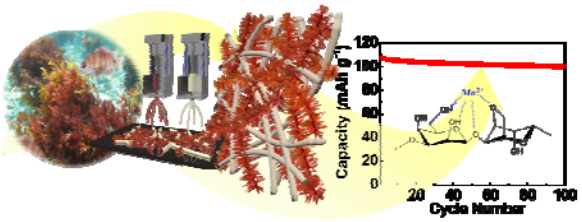

The agarose-biofunctionalized, dual-electrospun heteronanofiber mat was demonstrated as a new class of chemically-acitve (specifically, metal-ion chelating) battery separator membrane. The agrose-mediated Mn^{2+} chelation ability of the heteronanofiber mat separator, in association with its highly-porous structure and exceptional electrolyte wettability, enabled unprecedented improvement in the rate performance and high-temperature cyclability far beyond those achievable with conventional separators.